ISSN 0869-5911, Petrology, 2012, Vol. 20, No. 5, pp. 450–466. © Pleiades Publishing, Ltd., 2012.
Original Russian Text © E.V. Koptev-Dvornikov, N.S. Aryaeva, D.A. Bychkov, 2012, published in Petrologiya, 2012, Vol. 20, No. 5, pp. 495–513.

Equation of Thermobarometer for Description of Sulfide–Silicate Liquid Immiscibility in Basaltic Systems

E. V. Koptev-Dvornikov, N. S. Aryaeva, and D. A. Bychkov

Geological Faculty, Moscow State University, Moscow, 119991 Russia

e-mail: ekoptev@geol.msu.ru

Received December 21, 2011; in final form, February 27, 2012

Abstract—In order to describe sulfide–silicate liquid immiscibility, coefficients and constants in sulfide thermobarometer equation $X_S = \mathrm{EXP}(A/T - \beta P/T - B - CT - D\log f_{O_2} - \Sigma J_i X_i)$ were determined by multidimensional statistic analysis of a data set of more than 200 quench experiments on the solubility of sulfide sulfur in dry basaltic melts. Experiments characterize the sulfide–silicate equilibrium in a wide range of compositions, temperatures (1115–1800°C), pressures (1 atm–90 kbar) and oxygen fugacities ($\log f_{O_2}$ from −3.7 to −12.2). The average difference between experimental and calculated values of sulfur contents in sulfide-saturated basaltic melts is close to zero (0.0006 mol %), which indicates the absence of a systematic shift. The values of 5% confidence interval are described by equation $\pm(0.415C_S^2 - 0.211C_S + 0.038)$ (C_S in mol %) and fall within the range from ±0.012 to ±0.076 mol %. Proposed thermobarometer is presently a single thermobarometer that provides accuracy better than ±10 rel % of sulfur content, not logarithmic contents, within concentration range of 0.1–0.7 mol %. Verification of the thermobarometer on the basis of layered intrusion data showed that the proposed thermobarometer predicts the position of cumulus sulfide in the vertical sections of the Tsipringa and Kivakka intrusions with an accuracy of ±70 meters. At the same time, the reliable local prediction of layering-associated low-sulfide mineralization is impossible in the framework of model with ideal convective magma mixing in a chamber.

DOI: 10.1134/S0869591112050050

INTRODUCTION

Most of magmatogenic sulfide deposits are spatially and genetically related to mafic and ultramafic layered intrusions and represent the main sources of PGM, copper, and nickel. Most of researchers believe that they are generated due to magma splitting into immiscible silicate and sulfide liquids (Cawthorn, 1996; Naldrett, 2003). Separated sulfide liquid is capable of accumulating copper, nickel, and noble metals. No reliable criteria have been developed yet for local predicting the low-sulfide PGM mineralization. This problem can be solved by quantitative modeling of the formation of the inner structure of the massifs. The only computational tool to study of the solidification dynamics of the layered intrusions and to reproduce the distribution of rock-forming and trace elements in their vertical section is the COMAGMAT program (Ariskina and Barmina, 2000; Frenkel et al., 1988). The dynamic block of the program simulates crystal settling against convective stirring of the melt. However, this program in its present day form does not simulate the formation of rhythmic layering and associated low-sulfide mineralization.

The urgent problem is the development of a new model of the dynamics of layered intrusions simulating rhythmic layering and conjugate magmatogenic ore formation. The CryMinal program (Bychkov and Koptev-Dvornkov, 2005) (program of calculating the equilibrium CRYstallization of silicate system using a sum of mineral MINALs (end members) as an objective function) is the precursor of the thermodynamic block for a new multilayer-suspension model (Bychkova and Koptev-Dvornikov, 2004). For this thermodynamic block, we obtained liquidus thermobarometers (Koptev-Dvornikov et al., 2009) for rock-forming minerals of mafic rocks (olivines, plagioclase, augite, and orthopyoxene). These thermobarometers have the following forms:

$$\ln K = \frac{A + \beta P}{T} + B + CT + D\log f_{O_2} + E\ln\left(\frac{\mathrm{Al}}{\mathrm{Si}}\right) + FW + \sum_{i=1}^{n} J_i X_i, \quad (1)$$

where K is the constant of the reaction of the formation of end member (minal) of certain crystalline phase; P is the pressure in kbar, T is the absolute temperature, f_{O_2} is the oxygen fugacity, $W = \ln[(\mathrm{Na} + \mathrm{K})\mathrm{Al}/\mathrm{Si}^2]$, X_i is the mole fraction of i-th component of the melt, n is the number of incorporated components. The Al/Si and W parameters (calculated using atomic

proportions of elements) were proposed by (Ariskin and Barmina, 2000) to specify the olivine and plagioclase thermobarometers, respectively. A, β, C, D, E, F, and J_i are the coefficients for corresponding variables, B is the constant. These coefficients are calculated using multidimensional statistical methods. The thermodynamic sense of these constants follows from the view of the known physicochemical equations:

$$A \sim \Delta H/\mathrm{R},\ \beta \sim -\Delta V/\mathrm{R},\ \left\{ B + CT + D\log f_{\mathrm{O}_2} + E\ln\left(\frac{\mathrm{Al}}{\mathrm{Si}}\right) + FW + \sum_{i=1}^{n} J_i X_i \right\} \sim -\Delta S/\mathrm{R},$$

where ΔH, ΔV and ΔS are enthalpic, volumetric, and entropic effects of phase reactions, R is the universal gas constant. For each phase, we compiled a great body of experimental data, which characterizes the equilibrium of this phase with the melt, and using addins "solver" in MS Excel, determined the minimum of objective function. The objective function is the sum of squared difference between the experimental and calculated contents of corresponding end members, while optimized parameters are the coefficients and constant in equation (1). The equation for end members can be derived from equation (1) using reactions of their formation.

Thus, the trivial way to take into account the effect of variables (1) on the equilibrium constant led, however, to the quite satisfactorily result (Koptev-Dvornikov et al., 2009; Aryaeva, 2009). Obtaining statistically justified coefficients β is, in our opinion, of utmost importance, in spite of the low accuracy of high-pressure experiments. In this relation and in order to preserve the algorithmic uniformity of the KryMinal program, we attemped to apply equation (1) also to thermbarometer describing the sulfide–silicate liquid immiscibility (further, sulfide thermobarometer). Thus, in order to write sulfide barometer in clear form, it is necessary to determine the view of the reaction of the formation of liquid iron monosulfide from silicate melt.

A REVIEW OF PRESENTLY AVAILABLE REACTIONS OF THE FORMATION OF SULFIDE PHASE IN SILICATE SYSTEMS

A relatively limited number of possible phase reactions was proposed to describe the formation of sulfide liquid from silicate melt.

According to Wallace and Carmichael (1992), the reaction of heterogeneous equilibrium can be written as follows:

$$1/2\mathrm{S}_{2(\mathrm{gas})} + \mathrm{FeO}_{(\mathrm{sil})} = \mathrm{FeS}_{(\mathrm{sulf})} + 1/2\mathrm{O}_{2(\mathrm{gas})}. \quad (2)$$

Hereinafter, (sil) is silicate melt, (sulf) is sulfide melt.

The same reaction was used as basis for simulations of O'Neill and Mavrogenes (2002) and Li and Ripley (2009).

Liu et al. (2007) proposed the following reaction of sulfur dissolution in silicate melt:

$$\mathrm{FeS}_{(\mathrm{sulf})} + \mathrm{FeO}_{(\mathrm{sil})} + \mathrm{O}^{2-}_{(\mathrm{sil})} = \mathrm{S}^{2-}_{(\mathrm{sil})} + 2\mathrm{FeO}_{(\mathrm{sulf})}. \quad (3)$$

Poulson and Ohmoto (199) distinguished two regions of compositions of silicate melts (FeO > 10 wt % and FeO < 10 wt %), for which the chemical reactions of FeS solubility are described by different equations.

The compositional region FeO< 10 wt % was described by reaction:

$$\mathrm{FeS}_{(\mathrm{sil})} = \mathrm{FeS}_{(\mathrm{sulf})}. \quad (4)$$

For compositional region FeO > 10 wt %, they proposed the reaction of iron monosulfide formation, with participation of two FeO molecules, and sulfur existing as Fe_3SO_2 complex in silicate melt:

$$\mathrm{Fe_3SO_{2(sil)}} = \mathrm{FeS}_{(\mathrm{sulf})} + 2\mathrm{FeO}_{(\mathrm{sil})}. \quad (5)$$

Ariskin et al. (2008) developed this idea, suggesting that iron–sulfur complex in silicate melt has a variable composition. As in the work of Poulson and Ohmoto, the sulfide liquid immiscibility can be represented as result of decomposition of some "weighted average" complex:

$$(\mathrm{Fe}_z\mathrm{S})^{2(z-1)+}_{(\mathrm{sil})} = \mathrm{FeS}_{(\mathrm{sulf})} + (z-1)\,\mathrm{Fe}^{2+}_{(\mathrm{sil})}, \quad (6)$$

where z is the average size of clusters depending on the FeO content in silicate melt. The calculation of z parameter is yet unpublished special procedure.

Reaction (2) is presumably suitable for description of sulfide–silicate immiscibility under experimental conditions, when oxygen and sulfur fugacities are independent parameters defined by corresponding buffers, but it is hardy applied to the modeling of intrusive process solved in the framework of the KryMinal program.

Among other reactions that incorporate the components of condensed phases, we first studied the possibilities of the simplest reaction (4).

In this case $\ln K = \ln a_{\mathrm{FeS(sulf)}} - \ln a_{\mathrm{FeS(sil)}}$. Equation (1) is transformed in view:

$$\ln X_{\mathrm{S}} = -(A + \beta P)/T - B - CT - D\log f_{\mathrm{O}_2} - \Sigma J_i X_i, \quad (7)$$

since $a_{\mathrm{FeS(sulf)}}$ equals 1, while sulfur mole fraction in silicate melt X_{S} was taken as the simplest approximation for $a_{\mathrm{FeS(sil)}}$. Variables proposed by A.A. Ariskin and G.S. Barmina for olivine and plagioclase were omitted from equation (7).

Exponentiating equation (7) yields equation for X_{S}:

$$X_{\mathrm{S}} = \mathrm{EXP}(-A/T - \beta P/T - B - CT - D\log f_{\mathrm{O}_2} - \Sigma J_i X_i). \quad (7a)$$

Table 1. Characteristics of experimental data (204 experiments)

Number of experiments	Temperature range, °C	Pressure range, kbar	Oxygen fugacity range $\log f_{O_2}$	Reference
48	1200	0.001	from −8.86 to −11.09	(Haugton et al., 1974)
8	1200	0.001	from −10.5 to −11.5	(Buchanan, Nolan, 1979)
1	1450	0.001	−10.4	(Shima, Naldrett, 1975)
1	1400	0.001	−8.5	(Buchanan et al., 1983)
14	1115–1225	0.001–1	from −8.1 to −12.2	(Gorbachev, 1998)
28	1400–1800	5–90	from −3.66 to −10.96	(Mavrogenes, O'Neill, 1999)
26	1370–1600	9–27	from −8.86 to −10.29	(Holzhied, Grove, 2002)
29*	1400	0.001	from −9.6 to −10.92	(O'Neill, Mavrogenes, 2002)
13	1300–1335	10–16	from −7.58 to − 9.53	(Jugo et al., 2005)
36	1150–1450	5 and 10	from −7.34 to −9.79	(Liu et al., 2007)

Note: Among data (O'Neill and Marogenes, 2002), we excluded data lying beyond the limits of compositional polyhedron (Table 2) and results of FeS-undersaturated experiments.

DERIVATION OF EQUATION OF SULFIDE THERMOBAROMETER

Compilation of Experimental Data Set

Most of magmatogenic sulfide deposits are related to the mafic–ultramafic layered intrusions. Therefore, experiments performed with ultraacid, high-Ti, ultra-Al, ultra-Fe, and high-alkali melts were removed from data set on the FeS solubility in sulfide-saturated melts. Obtained set contains results of 204 experiments (Table 1).

Table 2. Range of contents of melt components in 204 experimental glasses (see Table 1)

Oxides	Range of contents, wt %
SiO_2	42.2–67.7
TiO_2	0–2.52
Al_2O_3	6.95–20.2
FeO	0.88–19.75
MnO	0–0.41
MgO	0–24.02
CaO	0–17.6
Na_2O	0–4.83
K_2O	0–2.74
P_2O_5	0–0.69
Cr_2O_3	0–0.416
S	0.022–0.401

All experiments were carried out under sulfide-saturated "dry" conditions. Oxygen fugacity for all experiments was below QFM (NNO-1), which provides the absolute predominance of sulfide sulfur over sulfate in "dry" conditions (for instance, see Fig. 8 in (Baker and Moretti, 2001) and Fig. 8 in (Wilke et al., 2011).

Thus, the obtained data set is characterized by the following range of conditions and compositions (Tables 1, 2, Fig. 1): temperature from 1115°C to 1800°C, pressure from 1 atm to 90 kbar, and oxygen fugacity $\log f_{O_2}$ from −3.66 to −12.2. All characteristics of these experiments used for calibrating equations are available from the authors upon request on ekoptev@geol.msu.ru.

Multidimensional Analysis of Experimental Data and Statistical Characteristics of Found Solution

At first, linear equation (7) was calibrated using multidimensional linear regression. This procedure was used to minimize the difference between experimental and calculated values of *logarithms* of sulfur contents. The contents of manganese, phosphorus, and chromium oxides were ignored during processing due to their low contents. Recalculation of molar concentrations into a sum of molar amounts included sulfur, while molar amounts of tri- and monovalent elements were calculated for one-metal species, for instance, for $FeO_{1.5}$ and $NaO_{0.5}$. Precisely these species were used in COMAGMAT and KryMinal programs for calculating sum of network-forming and network-modifying cations and emulation of activities

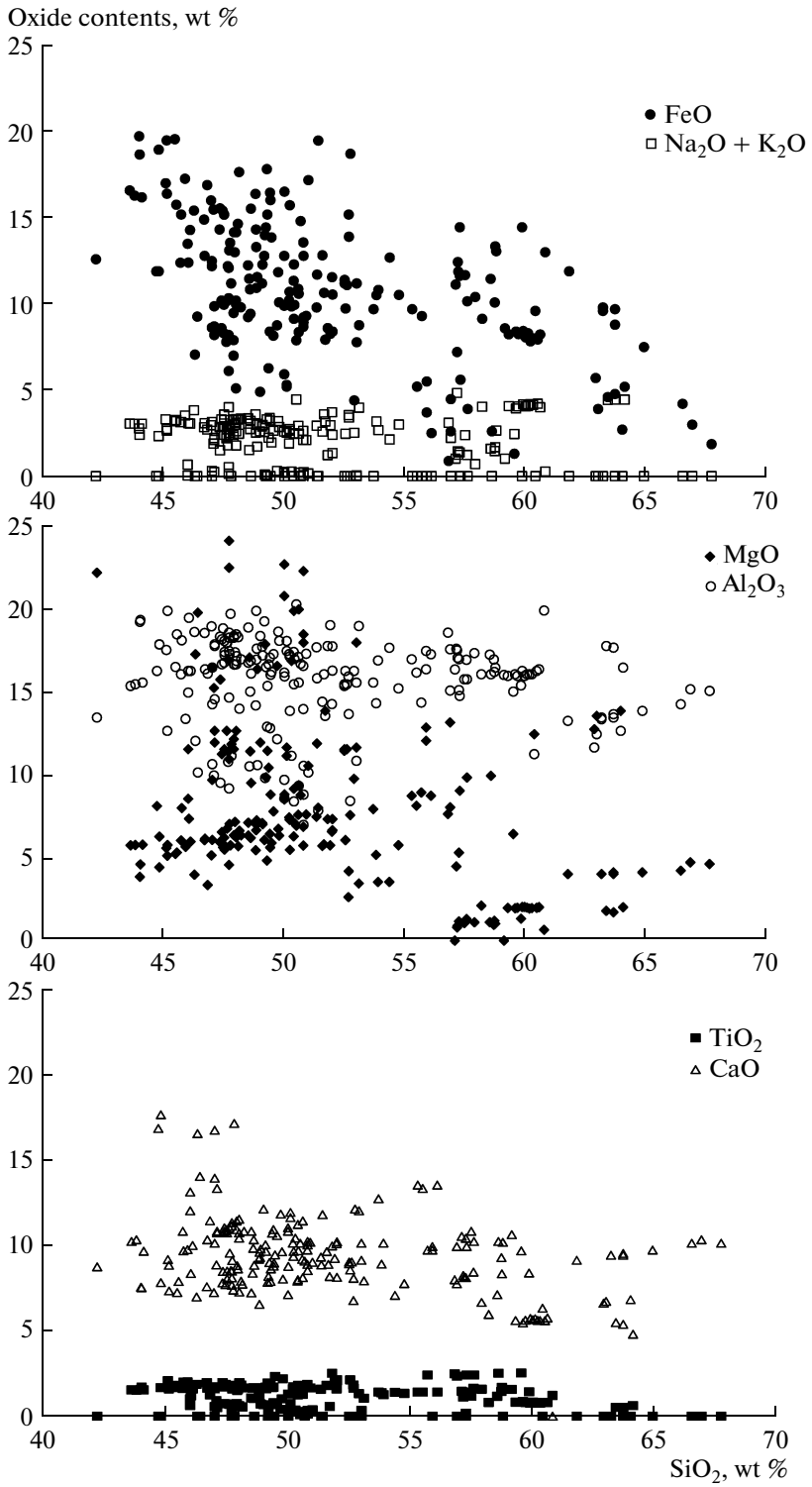

Fig. 1. Contents of oxides in experimental glasses that are in equilibrium with sulfide phase (204 experiments in data set). Distribution of compositions of experimental glasses within compositional polyhedron (Table 2) prevents appearance of false correlation in the course of statistical treatment.

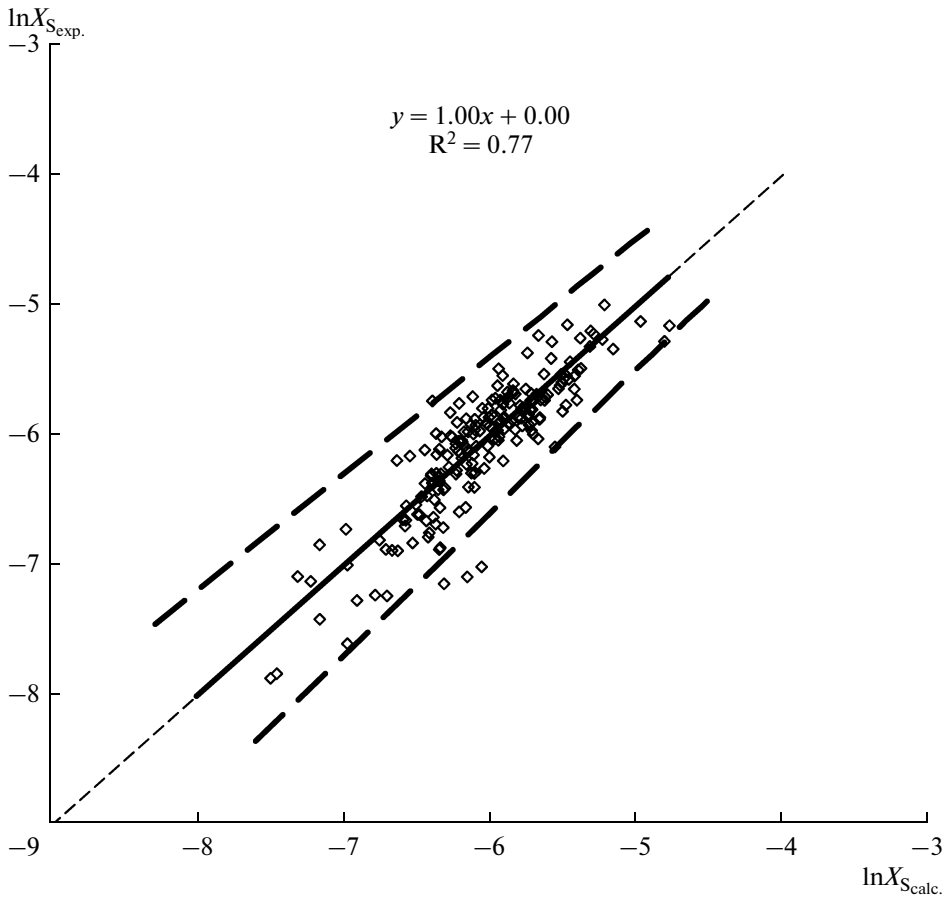

Fig. 2. Correlation between natural logarithms of calculated and experimental sulfur contents in sulfide-saturated basaltic melts (204 experiment in sampling). Solid line denotes linear trend, thin dashed line is the line of equal values (practically coincide), and bold dashed line denotes the boundaries of the corridor ±10 rel % of natural logarithms of sulfur contents.

of the components of silicate melts on this basis. Equation of (Killinc et al., 1983) was applied in order to divide total iron into ferric and ferrous iron. Obtained coefficients are presented in Table 3.

Traditional presentation of calibration results in the diagram in the logarithmic coordinates is shown in Fig. 2.

The result looks quite satisfactory: practically all data points fall in a "corridor" + 10% (relative) of natural logarithms of sulfur content, an equation of linear trend is ideal, and correlation coefficient is satisfactory.

However, substituting these coefficients in equation (7a) and analysis of relations of sulfur contents instead of its logarithms demonstrated unsatisfactory results (Fig. 3).

In this relation, we calibrated exponential equation (7a) using "solver" add-ins in MS Excel. The sum of squared differences between sulfur content in experimental glass and its calculated value was used as objective function. The minimum of the objective function corresponds to the optimal values of coefficients and constants. Among methods proposed in add-ins, the Newtonian optimization was chosen as the most rapid way.

Obtained coefficients and constants are listed in Table 3. They strongly differ from those for equation (7), while coefficients at direct and inverse temperatures appeared equal zero. It should be emphasized that the difference in coefficients is caused not by optimization method, but the choice of optimized parameter. The Newtonian optimization of squared difference of natural sulfur logarithms instead of their contents provides the same optimal values of coefficients and constants as those obtained by multidimensional linear regression.

The correlation between calculated and experimental sulfur contents in silicate melts in the presence of sulfide phase is shown in Fig. 4.

A cloud of data points is distinctly elongated along line of equal values, with argument coefficient equal 1 in the equation of linear regression in the plot (Fig. 4), while a free term equals 0. The differences between experimental and calculated values of sulfur contents show normal distribution. This is clearly demonstrated by histogram (Fig. 5).

The analysis of parameters used in our data set showed that none of variables in equation (7a) has normal or subnormal distribution and shows correlation with individual difference between experimental and calculated values. Hence, the differences between experimental and calculated values can be considered as random deviations from calculated values caused by analytical errors, deviations from equilibrium, measurement errors of experimental parameters, and others. The average deviation is close to zero amounting 0.0006 mol %, which indicates the absence of a systematic shift. It is seen in Fig. 4 that sulfur solubility for different concentrations is unevenly studied, therefore all range of sulfur contents was subdivided into 0.1 mol % segments and confidence interval was calculated for each segment. The boundaries of 5% confidence interval are described by equation $\pm(0.415C_S^2 - 0.211C_S + 0.038)$ (C_S, in mol %) and fall within a range from ±0.01 to ±0.05 mol % (Fig. 4). In spite of the fact that most of experimental points lie beyond confidence interval, the true measurable value (in our case, sulfur concentration in sulfide-saturated melt) lies within this narrow range within 95% probability. This results from statistical rule stating that results of similar reliability and measurement accuracy can be obtained using either a limited number of its high-pre-

Table 3. Values of coefficients and constants found using method of multidimensional linear regression for linear equation [7] and add-ins "Solver" in MS Excel for exponential equation (7a)

Coefficients and constants	Equation	
	(7)	(7a)
A	**−11189.35** (±33 rel. %)	**0**
b	**48.690135** (±10 rel. %)	**36.2351**
B	**−100.64035** (±10 rel. %)	**−79.2856**
C	**−0.0044535** (±30 rel. %)	**0**
D	**−0.1278735** (±21 rel. %)	**−0.13360**
J_{Si}	**121.32235** (±9 rel. %)	**85.3873**
J_{Ti}	**117.75535** (±9 rel. %)	**70.1940**
J_{Al}	**117.10535** (±9 rel. %)	**84.3308**
$J_{Fe^{3+}}$	**157.14035** (±9 rel. %)	**120.747**
$J_{Fe^{2+}}$	**115.23435** (±10 rel. %)	**78.0160**
J_{Mg}	**119.29135** (±9 rel. %)	**83.2915**
J_{Ca}	**117.99735** (±9 rel. %)	**81.5042**
J_{Na}	**124.65635** (±9 rel. %)	**88.7706**
J_K	**132.29935** (±10 rel. %)	**89.7324**

Note: Numbers in parentheses show standard error for coefficients, in relative percents.

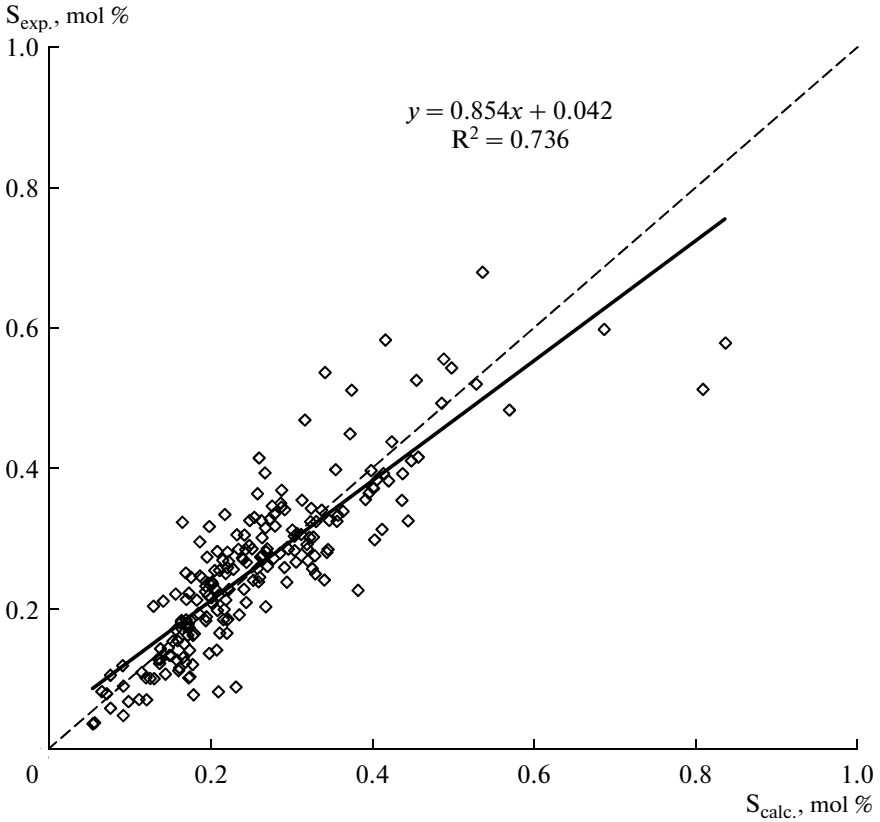

Fig. 3. Correlation between calculated and experimental sulfur contents in FeS-saturated silicate melts (204 experiments in data set). Results for equation (7a) with coefficients for equation (7) from Table 3. Solid line shows linear trend, thin dashed line is the line of equal values.

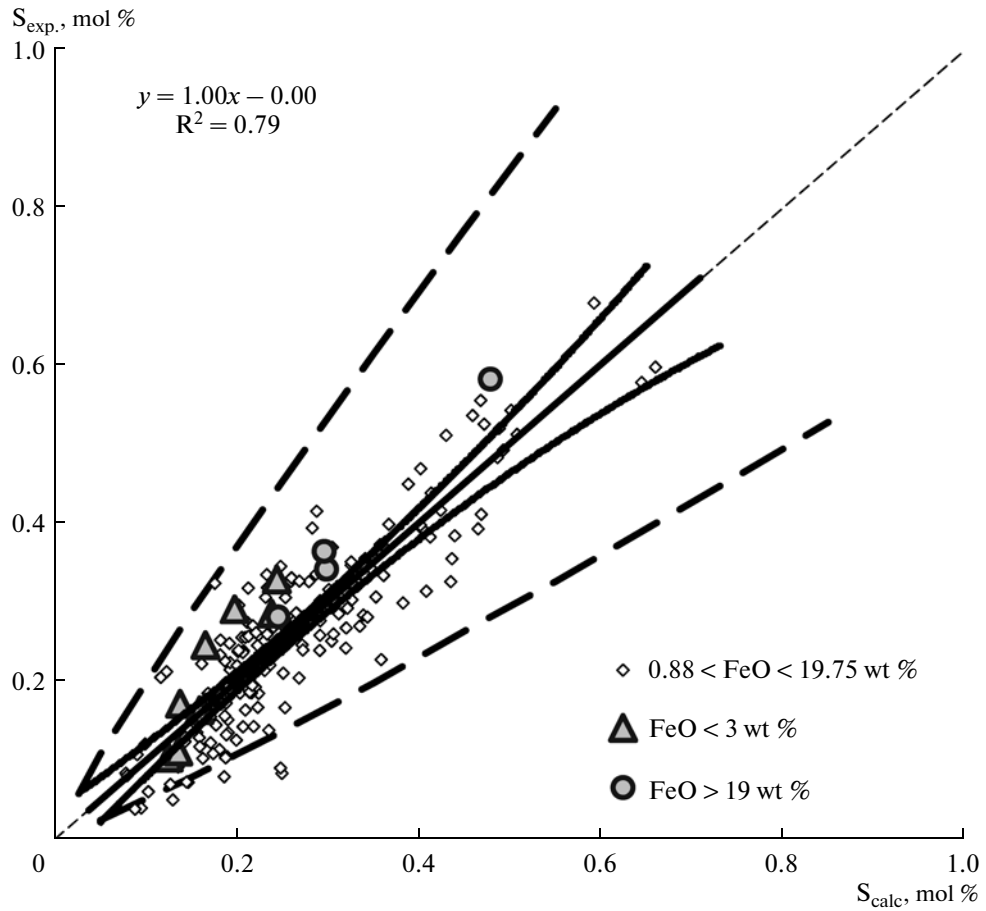

Fig. 4. Correlation between calculated and experimental sulfur contents in the FeS-saturated silicate melts (204 experiments in data set). Results for equation (7a) with coefficients from Table 3. Solid line is the linear trend, and thin dashed line is the line of equal values (practically coincide), bold curves are the boundaries of 5% confidence interval, and bold dashed lines are exponentiated boundaries of corridor ±10 rel. % of natural logarithms of sulfur content. See text for discussion.

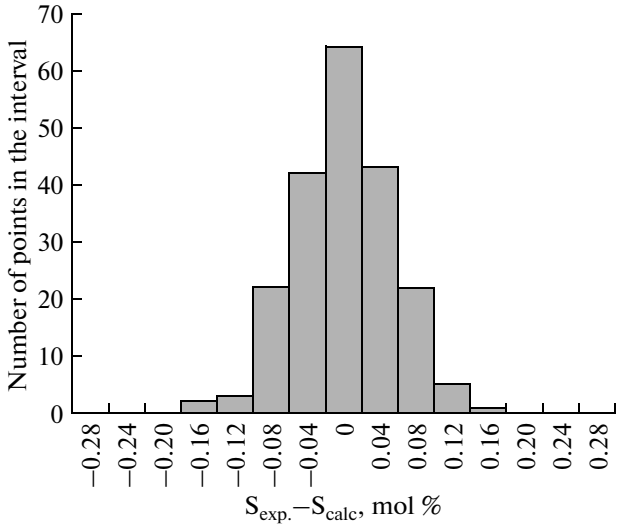

Fig. 5. Histogram of differences between experimental and calculated sulfur contents in FeS-saturated silicate melts (204 experiments in data set). Results for equation (7a) with coefficients from Table 3. Data show normal distribution.

cision measurements or a great number of measurements of low accuracy. Precisely a great number of treated experimental data allowed us to obtain such narrow confidence intervals.

Thus, in spite of the relatively wide scatter of data points around the trend in (Fig. 4), the great volume of data set made it possible to obtain sufficiently satisfactory results. This indicates that equation (7a) based on reaction (4) more satisfactorily reproduces experimental data within the entire range of composition, temperature, pressure, and oxygen fugacities. In spite of the fact that reaction (4) was proposed by Poulson and Ohmoto (1990) for silicate melts containing less than 10% FeO, but more than half (57%) of experimental melts in used set contains more than 10 wt % FeO, it is seen in Fig. 4 that high- and low-Fe experiments are equally well reproduced and even overlapped in the common graph.

Reviewing fifty-year researches on modeling sulfur solubility in magmas, Baker and Moretti (2011) arrived at a common understanding of mechanisms of sulfur dissolution in compositionally close silicate

Table 4. Values of confidence intervals for equation (7a) (in parentheses for equation (8b) and exponentiated boundaries of corridor ±10 rel. % of natural logarithms of sulfur contents

Range of sulfur contents, mol %	5% confidence interval, mol %	5% confidence interval, rel. %	Exponentiated boundaries of corridor ±10 rel. % of natural logarithms of sulfur content	Exponentiated boundaries of corridor ±10 rel .% of natural logarithms of sulfur contents
0.0–0.1	**±0.029** (±0.053)	**±58** (±103)	+0.027	+53
			–0.057	–114
0.1–0.2	**±0.014** (±0.020)	**±9** (±14)	+0.072	+48
			–0.137	–92
0.2–0.3	**±0.012** (±0.014)	**±5** (±6)	+0.113	+45
			–0.205	–82
0.3–0.4	**±0.014** (±0.023)	**±4** (±7)	+0.151	+43
			–0.266	–76
0.4–0.5	**±0.028** (±0.064)	**±6** (±14)	+0.188	+42
			–0.322	–72
0.5–0.6	**±0.046** (±0.122)	**±8** (±22)	+0.223	+41
			–0.375	–68
0.6–0.7	**±0.076** (±0.204)	**±12** (±31)	+0.257	+40
			–0.426	–65

melts and proposed both empirical and thermodynamic models for calculating sulfur contents in the sulfide-saturated melts. However, none of these models is perfect and their accuracy on the average is ±10 rel %. Nevertheless, such accuracy, according to these authors, is sufficient for many petrological studies and may constrain the boundaries for sulfur evolution in magmatic systems.

This conclusion is obviously misunderstanding. Judging from text and figures in cited publication and other works, authors implies ±10 rel. % of not sulfur content, but *logarithms* of its contents. Exponentiating the coordinates of these boundaries (bold dashed curves in Fig. 4) showed that the field between these boundaries coincides with the size of confidence interval only for the lowest sulfur contents. In other range of contents, the corridor ±10 rel. % of logarithmic contents is much wider than 5% confidence interval provided by our equation. The boundaries of ±10 rel. % of the logarithms of the sulfur contents provide uncertainty of predicted sulfur contents within limits indicated in Table 4 (two right columns). It is hardly possible that such an "accuracy" is sufficient for petrological and geochemical studies.

The relative size of confidence intervals for our equation is ±58 rel. % only for values X_S less than 0.1 mol %, and lies between ±4 and 12 rel. % at higher concentrations (Table 4).

Thus, the prediction of sulfur contents in silicate melts under sulfide saturation conditions ±10 rel. %, which is reported by Baker and Moretti (2011), can be provided only by our equation for dry basaltic systems within sulfur contents from 0.1 to 0.7 mol %. It is highly possible that the corresponding calibration of exponential equations for X_S instead of nonlinear logarithmic equations also will provide quite good accuracy of other equations. However, it is early to discuss this before conducting such procedures.

It should be noted that the accepted criterion to estimate quality of such thermobarometers by amount of experimental points falling in the interval ±10% of calculated values is incorrect. This interval is determined by a spread of distribution, which, in turn, depends not only on quality of processing, but mainly on integral error in instrumental and analytical measurements. Preserving distribution characteristics that are determined by experimental and analytical technologies, the number of points lying in the interval ±10% does not change with increasing number of measurements.

As an example, we calibrated one of the most popular equations of sulfur solubility under sulfide saturation conditions proposed by (Li and Ripley, 2009) using our data set. This equation has the following view:

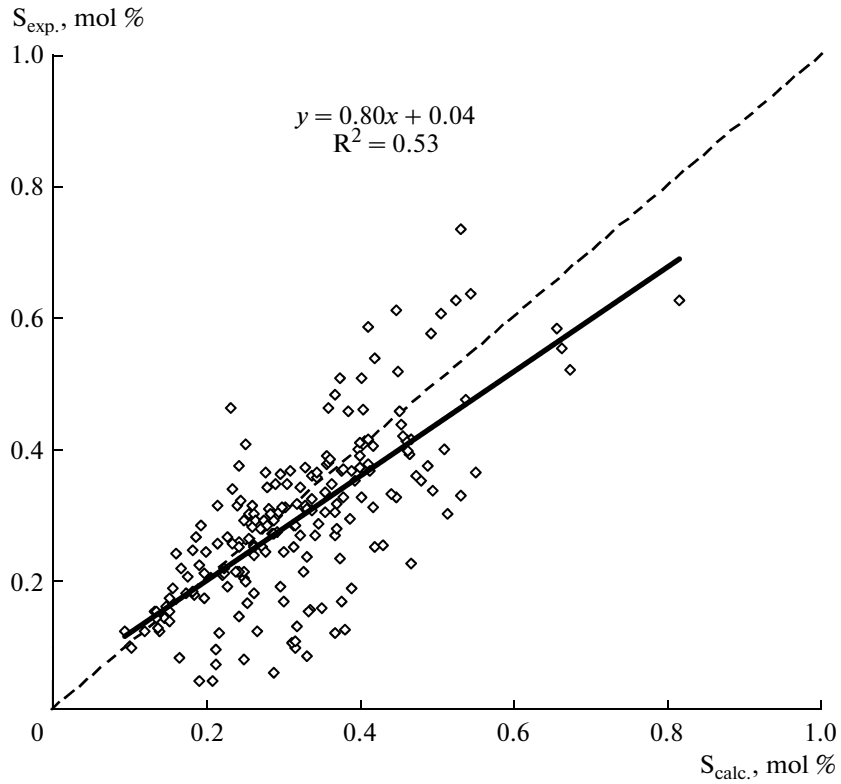

Fig. 6. Correlation of calculated and experimental sulfur contents in FeS-saturated silicate melts (204 experiments in data set). Result for equation (8a) from (Li and Ripley, 2009). Solid bold line is the linear trend, thin dashed line is the line of equal values.

$$\ln X_S = -1.76 - 0.474(10^4/T) - 0.021P + 5.559X_{FeO} + 2.565X_{TiO_2} + 2.709X_{CaO} - 3.192X_{SiO_2} - 3.049X_{H_2O}. \quad (8)$$

Transforming equation (8) into exponential form (8a),

$$X_S = \mathrm{EXP}\,(-1.76 - 0.474(10^4/T) - 0.021P + 5.559X_{FeO} + 2.565X_{TiO_2} + 2.709X_{CaO} - 3.192X_{SiO_2} - 3.049X_{H_2O}), \quad (8a)$$

we used values of coefficients and constants proposed by Li and Ripley for calculating X_S in our data sets. Results shown in Fig. 6 cannot be accepted as satisfactory and thus, coefficients and constants from equations (8) and (8a) are not suitable for our sampling. Note that while testing these equations, the weight contents of silicate melts were recalculated to molar concentrations according to scheme taken from (Li and Ripley, 2005).

Further, using add-ins "solver" in MS Excel program, we found the values of coefficients for variables and constants in the exponential equation (8a) for our data set. Since used experiments were conducted under "dry" conditions, the coefficient for X_{H_2O} was not optimized. The equation was transformed into:

$$X_S = \mathrm{EXP}\,(-1.93 - 0.571(10^4/T) - 0.021P + 5.617X_{FeO^-} - 2.793X_{TiO_2} + 2.410X_{CaO} - 2.055X_{SiO_2}). \quad (8b)$$

The results of calculation of sulfur contents are presented in Figs. 7 and 8.

They are much better than those for equation (8a). The parameters of linear trend are almost similar to those in Fig. 4, however, the correlation coefficients are significantly lower, and width of confidence intervals is significantly wider (Table 4).

The fact that equation (8b) yielded worse results than those of proposed thermobarometer can be explained by the fact that equation (7a) takes into account the pressure effect in the form of P/T variable having thermodynamic sense and depends on the great number of rock-forming oxides.

Thus, the sulfide thermobarometer (equation 7a) based on reaction (4) better fits experimental data than equation proposed by (Li and Ripley, 2009), at least in the region of dry basaltic melts.

We suggest that all already proposed and yet developed equations should be calibrated not in logarithmic but in exponential coordinates. It is more reasonable

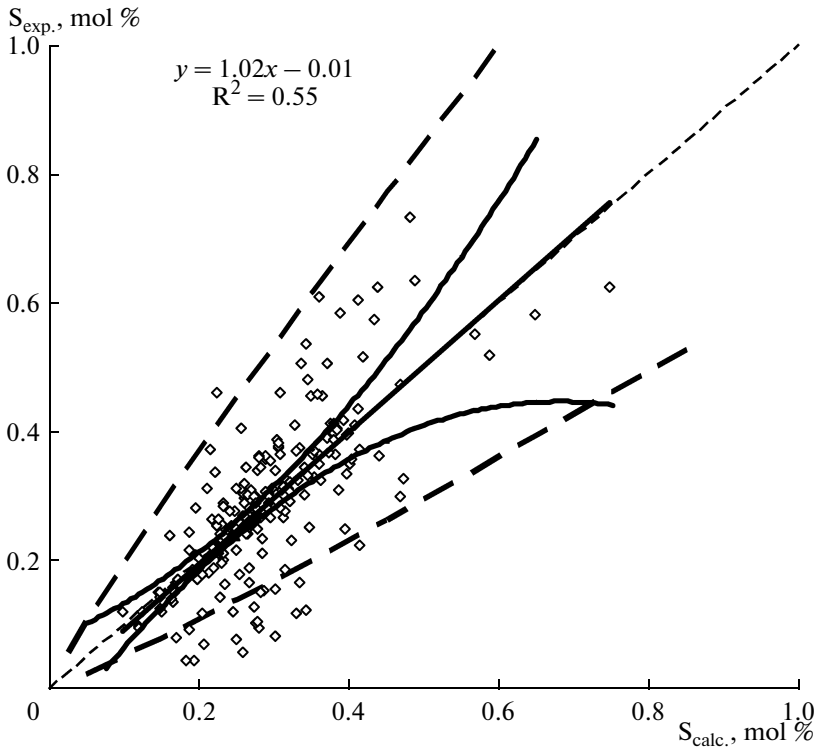

Fig. 7. Correlation between calculated and experimental sulfur contents in FeS-saturated silicate melts (204 experiments in data set). Result for equation (8b) optimized using add-ins "Solver" in MS Excel. Solid line is linear trend, thin dashed line is the line of equal values (practically coincide), while bold curves denote the boundaries of confidence interval at 5% significance level, bold dashed curves are exponentiated boundaries of corridor ±10 rel. % of natural logarithms of sulfur content.

to use the confidence interval at set significance level instead intuitive corridor ±10 rel. % of calculated value (why not 8 or 13%) as criterion.

We do not believe that obtained results may serve as evidence for the plausibility of reaction $FeS_{(sil)} = FeS_{(sulf)}$ for separation of sulfide melt from silicate melt. However, it is impossible not to admit that the reaction-based formalism with high accuracy reproduces experimental data.

This result will be more understandable if the process will be considered as the dissolution of iron monosulfide in silicate melt instead of formation of sulfide liquid from silicate melt. From this view point, precisely FeS goes into silicate melt, and the life of this molecule in silicate melt is not important, as was shown by approach applied in this work.

VERIFICATION OF SULFIDE THERMOBAROMETER

Data on the evolution of sulfur content in a melt during formation of magmatic object and sulfur contents calculated from equation (7a) with coefficients taken from Table 3 are required to verify the equation. The intersection of these curves marks the onset of sulfide–silicate liquid immiscibility in a magmatic chamber. In order to calculate sulfide contents required to trigger liquid immiscibility in the series of silicate residual melts, it is necessary to know the compositional evolution of these silicate melts. As in other cases, the large layered intrusive complexes represent

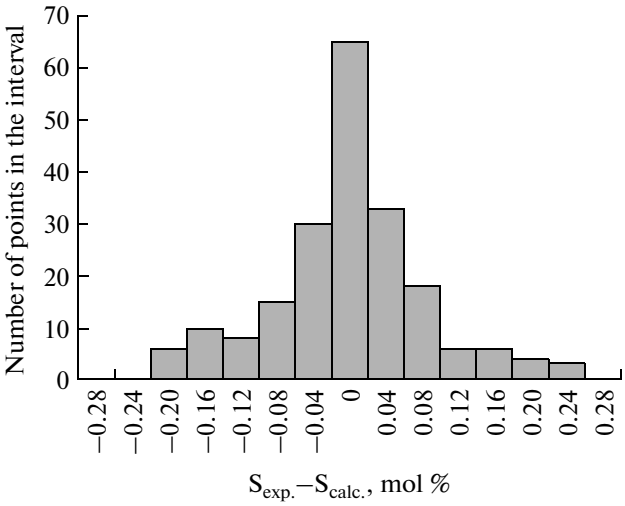

Fig. 8. Histogram of differences between experimental and calculated (on equation (8b)) sulfur contents in FeS-saturated silicate melts (204 experiments in data set). Normal distribution.

Table 5. Estimation of compositions of primary magmas for the Kivakka and Tsipringa intrusions

Components	1	2	3
SiO_2	51.29	49.82	49.82
TiO_2	0.31	0.23	0.58
Al_2O_3	11.57	12.53	17.92
FeO	9.28	8.83	10.37
MnO	0.19	0.16	0.15
MgO	17.91	18.24	8.17
CaO	7.99	8.41	9.73
Na_2O	1.15	1.52	2.73
K_2O	0.20	0.23	0.46
P_2O_5	0.10	0.02	0.06

Note: (1) Average composition of the rocks of the bottom facies of the Kivakka Intrusion (Lavrov, 1979); (2) weighted average composition of the Kivakka intrusion after (Koptev-Dvornikov et al., 2001); (3) weighted average composition of the Tsipringa intrusion after (Semenov et al., 1995).

suitable objects for testing genetic considerations. In that case, data on compositional variations of the melt, including sulfur content, during solidification of intrusion can be obtained by means of developing optimal model of the intrusion formation. Preliminary verification was carried out by modeling in the COMAGMAT program (Ariskin and Barmina, 2000; Frenkel, 1995; Frenkel et al, 1988). In turn, in order to obtain distributions of rock-forming oxides and trace elements (including sulfur) required for testing model calculations and to estimate the composition of parental magma, it is necessary to sample in detail the vertical section of the intrusion with accurate assignment of samples to the vertical coordinate of the section. The weighted average composition of the intrusion is used as estimated composition of parental magma. The onset of liquid immiscibility is marked by the distribution of chalcophile elements (in our case, Cu), whose maximums correspond to the position of low-sulfide horizons in the massif section.

Remember that COMAGMAT program simulates cooling intrusion and settling of crystallizing phases via ideally convectively stirring magma in a closed chamber, which is attained by postulating of temperature, phase, and chemical homogeneity of magma between the upper solidification boundary and cumulus surface in each moment of time. This prevents us from modeling rhythmic layering. Hence, equation (7a) is more preferable for verification of layered intrusion with weakly pronounced rhythmicity and single manifestation of low-sulfide horizon in the section. Such intrusions are few in number, and can be exemplified by the Tsipringa troctolite–gabbronorite massif in North Karelia (Semenov et al., 1995).

Carried out studies allowed us to give the detailed description of the inner structure of the Tsipringa intrusion and to quantify the evolution of rock composition in its vertical section. It was established that the massif represents a typical in situ layered intrusion of lopolithic shape 3100 m thick, the southern and northern boundaries of which initially represented its lower and upper contacts. The weighted average composition of the intrusion corresponds to aluminous tholeiitic basalts (Table 5).

Obtained quantitative characteristics of the intrusion (its thickness, composition of primary magma, and distribution of major and trace elements throughout the intrusion) are sufficient for numerical modeling of solidification dynamics.

Based on the distribution of rock-forming minerals in vertical cross-section of the massif, the following order of its crystallization can be proposed: a short crystallization period of excess plagioclase, long-term (judging from thickness of this area) crystallization stage of plagioclase–olivine cotectics, during which meso- and leuctroctolite sequence was formed. Overlying olivine–plagioclase–augite cumulates mark the appearance of liquidus clinopyroxene. Upsection, the rocks contain cumulus pigeonite and lack olivine. The sequence is crowned by plagioclase–augite–pigeonite–Ti-magnetite cumulates with low-sulfide horizon at the base.

Thus, the following crystallization order of primary magma can be determined: plagioclase $\longrightarrow$ olivine + plagioclase $\longrightarrow$ olivine + plagioclase + augite $\longrightarrow$ plagioclase + augite + pigeonite(– olivine) $\longrightarrow$ plagioclase + augite + pigeonite + magnetite. Such a crystallization order is typical of the tholeiitic magmas with appearance of liquidus low-Ca pyroxene after augite and with crystallization of pigeonite as low-Ca pyroxene.

Simulation was carried out using COMAGMAT program version 3.5 (Frenkel, 1995; Ariskin and Barmina, 2000; Frenkel et al., 1988). The weighted average composition of the intrusion was taken as primary magma composition (Table 5). The aforementioned crystallization order is best simulated at pressure of 5 kbar. Varying the settling rates and fractions of residual melt entrapped by cumulus provides quantitative agreement between natural and model distributions of minerals throughout the section (Fig. 9).

Using model data on the compositional evolution of residual melts, their temperature, pressure and oxygen fugacity, we calculated the sulfur content required to start the separation of sulfide phase. A sharp increase in the content of chalcophile elements, according to data of N.F. Pchelintseva (Semenov et al., 1995) in the rocks at a height of 2300 m from the intrusion base corresponds to the unmixing of sulfide liquid in the intrusive chamber and formation of low-

Fig. 9. Natural and model distributions of rock-forming minerals in the vertical cross-section of the Tsipringa Intrusion. (*Ol*) olivine, (*Pl*) plagioclase, (*Cpx*) clinopyoxene, (*Opx*) orthopyroxene.

sulfide mineralization (Fig. 10). The same figure shows the evolution of sulfur content in the residual melt with crystallization of primary magma (according to data of numerical modeling) and change in sulfur contents required to trigger sulfide–silicate liquid immiscibility [calculated using equation (7a)].

It is seen that during the most part of the intrusion evolution, the sulfur content in the melt was lower than that required to reach liquid immiscibility. These curves intersected only when cumulus was formed at a height of 2300 m. This means that liquid immiscibility occurred and sulfide liquid began to fractionate precisely at the moment when cumulus surface reached this level. At the expense of confidence interval (±0.014 mol %), the appearance of cumulus sulfides within height range from 2170 to 2310 m should be expected at the 95% probability limit.

For comparison, Figure 10 demonstrates thin dashed curves, which bracket the width of the uncertainty interval set by exponentiated boundaries of the

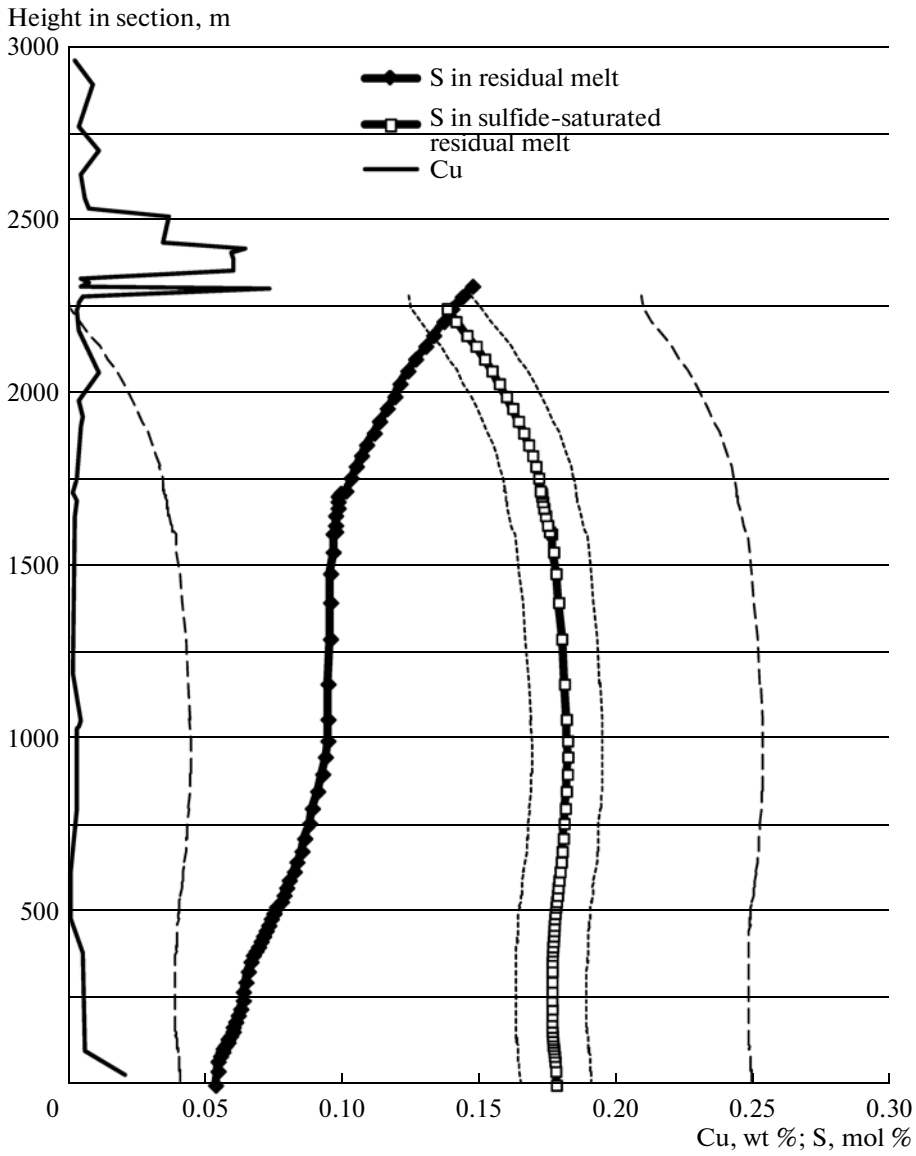

Fig. 10. Cu distribution in the vertical section of the Tsipringa intrusion, evolution of sulfur content in the residual melt with crystallization of primary magma and change of sulfur content in the sulfide-saturated residual melts, calculated using equation (7a). Thin dashed lines limit the width of confidence interval for sulfur concentration range of 0.1–0.2 mol % (Table 4), which with probability of 95% contain true sulfur content required to reach sulfide–silicate liquid immiscibility. Thin dashed curves constrain the width of uncertainty interval set by exponentiated boundaries of corridor of ±10 rel. % of natural logarithmic sulfur contents for range of sulfur contents within 0.1–0.2 mol % (Table 4).

corridor ±10 rel. % of natural logarithms of sulfur content for sulfur range of 0.1–0.2 mol % (Table 4). Such an "accuracy" is too low to predict the onset of sulfide–silicate liquid immiscibility in the intrusive chamber.

The efficiency of our sulfide thermobarometer for intrusion with developed rhythmic layering was estimated using data on the Kivakka olivinite–norite–gabbronorite intrusion (Lavrov, 1979; Koptev-Dvornikov et al., 2001; Bychkova and Koptev-Dvornikov, 2004), for which we have all required information, as for the Tsipringa Massif.

Based on the outlines of the intrusion, its initial shape may be interpreted as vertical inverted cone with an apex angle around 80° and height around 3.9 km (Koptev-Dvornikov et al., 2001). Later, the intrusion was inclined at angle of 36° to the northwest and eroded. The weighted average composition of the intrusion is close to that of the near-contact facies and corresponds to the basalts of the marianite–boninite series (Table 5). An order of change of cumulus assemblages along the vertical section reflects the crystallization order of initial magma: olivine ⟶ (–olivine) + orthopyroxene + plagioclase ⟶ orthopyroxene + plagioclase + clinopyroxene ⟶ (–orthopyroxene) +

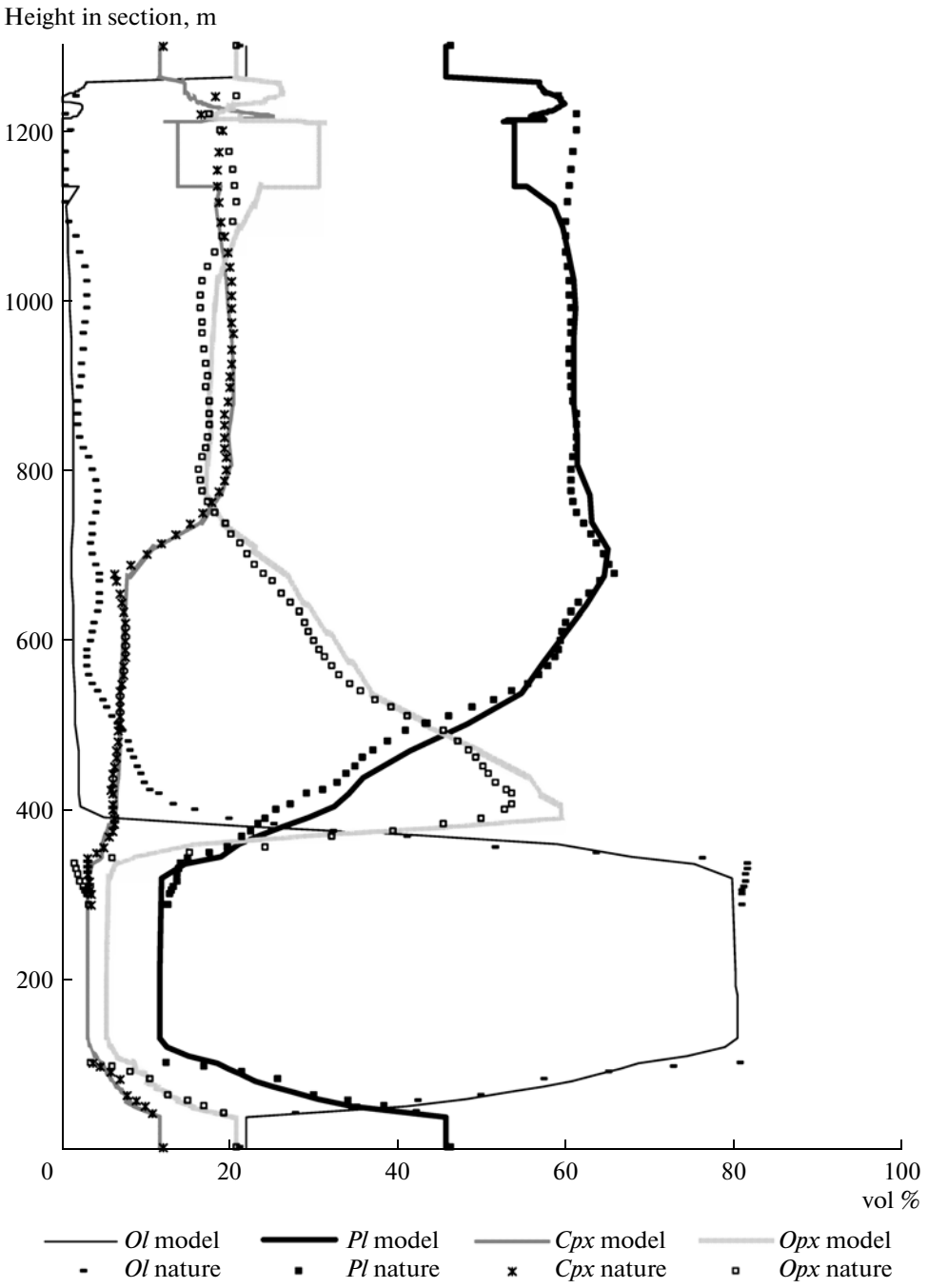

Fig. 11. Natural and model distributions of the rock-forming minerals in the vertical section of the Kivakka intrusion. (*Ol*) olivine, (*Pl*) plagioclase, (*Cpx*) clinopyroxene, (*Opx*) orthopyroxene.

clinopyroxene + plagioclase + pigeonite (sign minus denotes the incongruent dissolution of the phase). Such a succession of cumulus assemblages is typical of the intrusions derived from of boninite-like magmas (Bushveld, Sillwater, Monchegorsk, and others). Single difference is the absence of chromite among crystallization products in the Kivakka pluton.

Since COMAGMAT is unidimensional model and does not allow modeling conical bodies, the section of conical intrusion was recalculated for cylindrical shape with the preservation of the total volume of the massif and volumes of derivatives. The thickness of this cylinder was 1300 m (Fig. 11). The rhythmic layering is observed between 360 to 680 meters, and bear contrasting character (different cumulus assemblages in the alternating layers) from 360 to 510 m (Bychkova and Koptev-Dvornikov, 2004). Upward, the layering is

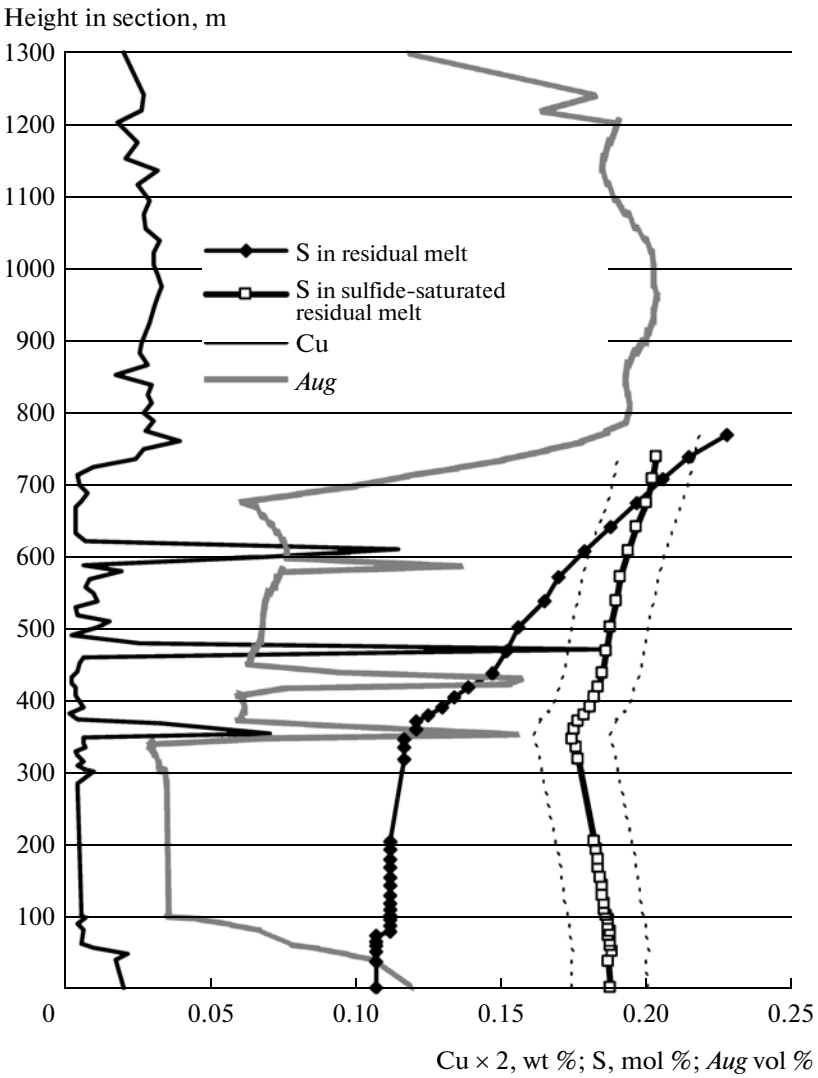

Fig. 12. Distribution of copper and augite in the vertical section of the Kivakka intrusion, evolution of sulfur content in the residual melt with crystallization of primary magma and change of sulfur content in the sulfide-saturated residual melts calculated using equation (7a). Thin dashed line constrain the width of confidence interval for sulfur concentrations within 0.1–0.2 mol % (Table 4), which with a 95% probability contains true sulfur content required to reach sulfide–silicate liquation. (*Aug*) augite.

mainly expressed by variations in the mafic index of the rocks.

Modeling was carried out using COMAGMAT program version 3.5. Since rhythmic layering cannot be simulated using COMAGMAT program, the primary distributions of chemical elements and minerals were smoothed using sliding windows for verification of model calculations. In order to avoid the blurring between zones with different assemblages, each zone was smoothed separately up to elimination of high-frequency variations in rock composition. The weighted average composition of the intrusion was taken as the initial composition of magma (Table 5). The fact that plagioclase and othopyroxene become cumulus phases at the same level of vertical section (Fig. 11) indicates their simultaneous crystallization in the chamber. For taken composition of primary magma, this occurred at a pressure of 2.6 kbar. Varying the settling rates of minerals and fractions of residual melt entrapped by cumulus allowed us to fit natural distribution of minerals in the intrusive section (Fig. 11).

By analogy with Fig. 10, Figure 12 demonstrates the distribution of copper and sulfur contents in the residual melts and sulfur contents that are required to reach equilibrium between residual melts and iron monosulfide. Two segments are clearly distinguished in the copper distribution curve. In the lower part (up to 710 m), three copper peaks corresponding to the low-sulfide horizons associated with rhythmic layering are distinguished against the background of low (~0.005 wt %) copper contents. In the upper part of the section, the copper contents are steadily three times higher (~ 0.015 wt %); for better observation, the copper contents are multiplied by two (Fig. 12). The

prominence in concentrations corresponds to the moment of steady appearance of cumulus sulfide phase. It is noteworthy that numerical (COMAGMAT) modeling showed that the curves of sulfur content in the residual melt and its content required to reach liquid immiscibility are intersected precisely at this height. Due to the width of the confidence interval (±0.014 mol %), the appearance of cumulus sulfides should be expected with a 95% probability from 610 to 740 m. Thus, our thermobarometer also successfully predicted the moment of the onset of sulfide–silicate liquid immiscibility in the chamber of crystallizing intrusion for the Kivakka intrusion.

Practically constant copper contents from this level upward denotes that in spite of the sufficiently high copper partition coefficient between sulfide and silicate liquid (~ 800 (Pchelintseva and Koptev-Dvornikov, 2008), the combined coefficient is approximately 1. This allows us to estimate the weight fraction of sulfide liquid among other phases separated from silicate melt. It accounts for $\sim 1/K_D^{Cu}$, namely, $1/800 = 0.00125$.

However, COMAGMAT program postulating ideal stirring of convective magma in chamber does not provide information concerning localization of low-sulfide horizons, which are of economic interest in the layered intrusions. Figure 12 demonstrates one more curve: smoothed distribution of volumetric augite fraction in the vertical section. This curve reproduces the primary contents of clinopyroxene at three levels of its "premature" cumulus appearance in the gabbronorite layers among norite–bronzitite rhythmic alternation (Bychkova and Koptev-Dvornikov, 2004). A sharp increase in the clinopyroxene fraction observed in the rocks upsection at a height of 680 m corresponds to the steady appearance of augite in cumulus in nature and in liquidus in model. Note two facts: (1) sulfide–silicate liquid immiscibility occurs in the chamber soon after beginning of clinopyroxene crystallization; (2) low-sulfide horizons are spatially related to the gabbronorite horizons, but not always coincide with them. Hence, we may conclude with caution that the low-sulfide horizons in the rhythmically layered units are confined to those cumulates that demonstrate sulfide–silicate liquid immiscibility.

It is noteworthy that the content of sulfur as incompatible element increases in the residual melts of both the intrusions, whereas its content required to reach liquid immiscibility shows different behavior for the evolution of different magma types. The sulfur content required to trigger liquid immiscibility decreases with differentiation in the Tsipringa intrusion and increases in the Kivakka intrusion, but with a lower rate than sulfur content in the residual melt.

CONCLUSIONS

(1) It was shown that FeS solubility calculated on the basis of reaction proposed by (Poulson and Ohmoto, 1990) for low-Fe melts $\mathbf{FeS_{(sil)} = FeS_{(sulf)}}$ is suitable for wide compositional range of basaltic systems, temperatures (1115–1800°C), and pressures (1 atm–90 kbar) regardless of FeO content.

(2) Processing of a great body of experimental data by multidimensional statistics made it possible to obtain equation of sulfide thermobarometer, which with high accuracy describes the solubility in sulfide-saturated silicate melts. Proposed thermobarometer presently is a single tool providing accuracy ±10 rel. % of sulfur content (not of logarithms of contents) within concentration range of 0.1–0.7 mol %.

(3) All already proposed and yet developed equations of sulfide thermobarometers should be calibrated on exponential instead of logarithmic scale. The value of confidence interval at taken significance level should be used as criterion of accuracy instead of intuitive corridor ±10 rel. % (why not 8 or 13%?) of the value of studied parameter.

(4) Saturated sulfur concentrations calculated using numerical modeling of the formation of the Tsipringa and Kivakka layered intrusions satisfactorily predict the height of the appearance of cumulus sulfide phase in the intrusive chamber.

(5) Reliable local prediction of low-sulfide mineralization associated with rhythmicity is impossible in the framework of model with ideal convective magma stirring in a chamber.

ACKNOWLEDGMENTS

We are grateful to M.V. Borisov (Moscow State University), A.A. Ariskin (Vernadsky Institute of Geochemistry and Analytical Chemistry of RAS), A.A. Borisov (Institute of Geology of Ore Deposits, Petrography, Mineralogy, and Geochemistry of RAS), and S. A. Vorob'ev for interest in discussing the paper and useful comments.

The work was supported by the Russian Foundation for Basic Research (project no. 11-05-01027a).

REFERENCES

Ariskin, A.A. and Barmina, G.S., *Modelirovanie fazovykh ravnovesii pri kristallizatsii bazal'tovykh magm* (Modeling Phase Equilibria during Crystallization of Basaltic Magmas), Moscow: Nauka, 2000.

Ariskin, A.A., Bychkov, K.A., Danyushevsky, L.V., and Barmina, G.S., A Model of S Solubility in Basaltic Melts at 1 Atm, *Geochim. Cosmochim. Acta*, 2008, vol. 72 (Suppl. 1, Abs. 18th Annual Goldschmidt Conf., Vancouver, Canada, 2008, A31).

Aryaeva, N.S., Geothermometers Describing Crystallization of Silicates from Basic Magmas within Wide Composition and Pressure Range, in *Planeta Zemlya: aktual'nye voprosy geologii glazami molodykh uchenykh i studentov. Mater. ros. konf. stud., aspir. i mol. uch., posvyashchennoi "Godu Planety Zemlya"*, (Planet Earth: Actual Geological Problems as Viewed by Young Scientists and Students. Proceedings of

Russian Conference of Students, Post-Graduate Students, Young Scientists, devoted to the Planet Earth's Year), Moscow, 2009, vol. 2, pp. 8–11. http:/geo.web.ru/pubd//2009/04/14/0001182159/2_02.pdf

Baker, D.R. and Moretti, R., Modeling the Solubility of Sulfur in Magmas: a 50-Year Old Geochemical Challenge, *Rev. Mineral. Geochem.*, 2011, vol. 73, pp. 167–213.

Buchanan, D.L. and Nolan, J., Solubility of Sulphur and Sulphide Immiscibility in Synthetic Tholeiitic Melts and Their Relevance to Bushveld-Complex Rocks, *Can. Mineral.*, 1979, vol. 17, pp. 483–494.

Buchanan, D.L., Nolan, J., Wilkinson, N., and De Villiers, J.P.R., En Experimental Investigation of Sulfur Solubility As a Function of Temperature in Synthetic Silicate Melts, *Geol. Soc. South Afr., Sp. Publ.*, 1983, vol. 7, pp. 383–391.

Bychkov, D.A. and Koptev-Dvornikov, E.V., A KriMinal Program for Modeling Melt–Solid Phase Equilibria at Given Bulk Composition of the System, *Mater. mezhd. konf. "Ul'tramafit-mafitovye kompleksy skladchatykh oblastei dokembriya*, (Proc. Intern. Conf. "Ultramafic–Mafic Complexes of the Precambrian Folded Regions), Ulan-Ude, 2005, pp. 122–123.

Bychkov, K.A., Ariskin, A.A., Danyushevsky, L.V., and Barmina, G.S., Testing of Sulphide Solubility Models and Calculations of SCSS during Crystallization of Mafic Magmas Parental to Layered Intrusions, *Northwestern Geology*, vol. 42 (Suppl.) (Proc. Xi'an Intern. Ni–Cu (Pt) Deposit Symposium 2009), pp. 15–19.

Bychkova, Ya.V. and Koptev-Dvornikov, E.V., Rhythmic Layering of the Kivakka Type: Geology, Petrography, Petrochemistry, and a Hypothesis for Its Formation, *Petrology*, 2004, vol. 12, no. 3, pp. 244–264.

Frenkel, M.Ya., *Teplovaya i khimicheskaya dinamika differentsiatsii bazitovykh magm* (Thermal and Chemical Dynamics of Differentiation of Basic Magmas), Moscow: Nauka, 1995.

Frenkel, M.Ya., Yaroshevskii, A.A., Ariskin, A.A., et al., *Dinamika vnutrikamernoi differentsiatsii bazitovykh magm* (Dynamics of Intrachamber Differentiation of Basic Magmas), Moscow: Nauka, 1988.

Gorbachev, P.N., Experimental Study of Sulfur Solubility in the Basaltic Melts in Equilibrium with Sulfide Liquid, *Extended Abstract of Cand. Sci. (Geolmin) Dissertation*, Moscow: Moscow State University, 1998.

Haughton, D.R., Roeder, P.L., and Skinner, B.J., Solubility of Sulphur in Mafic Magmas, *Econ. Geol.*, 1974, vol. 69, pp. 451–466.

Holzhied, A. and Grove, T.L., Sulfur Saturation Limits in Silicate Melts and Their Implications for Core Formation Scenarios for Terrestrial Planets, *Am. Mineral.*, 2002, vol. 87, pp. 227–237.

Jugo, P.J., Luth, R.W., and Richards, J.P., An Experimental Study of the Sulfur Content in Basaltic Melts Saturated with Immiscible Sulfide or Sulfate Liquids at 1300°C and 1GPa, *J. Petrol.*, 2005, vol. 46, no. 4, pp. 783–798.

Killinc, C., Carmichael, I.S.F., Rivers, M., and Sack, R.O., The Ferric-Ferrous Ratio of Natural Silicate Liquids Equilibrated in Air, *Contrib. Mineral. Petrol.*, 1983, vol. 83, nos. 1–2, pp. 136–140.

Koptev-Dvornikov, E.V., Aryaeva, N.S., and Bychkov, D.A., Pressure Dependence of Crystallization Temperature and Composition of Rock-Forming Silicates of Basic Rocks: Multidimensional Statistic Processing of Experimental Data and Numerical Modeling, in *Mater. nauch. konf. "Lomonosovskie chteniya", sektsiya geologiya, podsektsiya geokhimiya* (Proc. Sci. Conf. "Lomonosov Reading'" Geological Section, Geochemical Subsection), Moscow, 2009. http:/geo.web.ru/pubd//2009/04/15/0001182162/ 26.pdf.

Koptev-Dvornikov, E.V., Kireev, B.S., Pchelintseva, N.F., and Khvorov, D.M., Distribution of Cumulative Mineral Assemblages, Major and Trace Elements over the Vertical Section of the Kivakka Intrusion, Olanga Group of Intrusions, Northern Karelia, *Petrology*, 2001, vol. 9, no. 1, pp. 3–27.

Lavrov, M.M., *Giperbazity i rassloennye peridotit-gabbro-noritovye intruzii dokembriya Severnoi Karelii* (The Precambrian Ultramafic and Layered Peridotite–Gabbro–Norite Intrusions of North Karelia), Leningrad: Nauka, 1979.

Layered Intrusions, Cawthorn, R.G., Ed., Amsterdam: Elsevier, 1996.

Li, C. and Ripley, E.M., Empirical Equations To Predict the Sulfur Content of Mafic Magmas at Sulfide Saturation and Applications to Magmatic Sulfide Deposits, *Miner. Deposita*, 2005, vol. 40, pp. 218–230.

Li, C. and Ripley, E.M., Sulfur Contents at Sulfide-Liquid Or Anhydrite Saturation in Silicate Melts: Empirical Equations and Example Applications, *Econ. Geol.*, 2009, vol. 104, pp. 405–412.

Liu, Y., Samaha, N.-T., and Baker, D.R., Sulfur Concentration at Sulfide Saturation (SCSS) in Magmatic Silicate Melts, *Geochim. Cosmochim. Acta*, 2007, vol. 71, pp. 1783–1799.

Mavrogenes, J.A. and O'Neill, H.St.C., The Relative Effects of Pressure, Temperature and Oxygen Fugacity on the Solubility of Sulfide in Mafic Magmas, *Geochim. Cosmochim. Acta*, 1999, vol. 63, pp. 1173–1180.

Naldrett, A.J., *Magmaticheskie sul'fidnye mestorozhdeniya medno-nikelevykh i platinometal'nykh rud* (Magmatic Sulfide Deposits of Nickel and PGE Ores), St. Petersburg: SPbGU, 2003.

O'Neill, H.S.C. and Mavrogenes, J.A., The Sulfide Capacity and the Sulfur Content at Sulfide Saturation of Silicate Melts at 1400°C and 1 Bar, *J. Petrol.*, 2002, vol. 43, pp. 1049–1087.

Pchelintseva, N.F. and Koptev-Dvornikov, E.V., On the Genesis of Platiniferous Low-Sulfide Rocks in the Kivakka Layered Intrusion, Northern Karelia, *Geochem. Int.*, 2008, no. 6, pp. 627–633.

Poulson, S.R. and Ohmoto, H., An Evaluation of the Solubility of Sulfide Sulfur in Silicate Melts from Experimental Data and Natural Samples, *Chem. Geol.*, 1990, vol. 85, pp. 57–75.

Semenov, V.S., Koptev-Dvornikov, E.V., Berkovskii, A.N., et al., Tsipringa Layered Troctolite–Gabbro–Norite Intrusion: Geological Structure and Petrology, *Petrologiya*, 1995, vol. 3, 1–23.

Shima, H. and Naldrett, A.J., Solubility of Sulphur in An Ultramafic Melt and Relevance of the System Fe–S–O, *Econ. Geol.*, 1975, vol. 70, pp. 960–967.

Wallace, P. and Carmachael, L.S.E., Sulfur in Basaltic Magmas, *Geochim. Cosmochim. Acta*, 1992, vol. 56, pp. 1863–1874.

Wilke, M., Klimm, K., C., and Kohn S.C. Spectroscopic Studies on Sulfur Speciation in Synthetic and Natural Glasses, *Rev. Mineral. Geochem.*, 2011, vol. 73, pp. 41–78.